https://doi.org/10.1016/j.jobe.2021.102975

A combined framework of integrating optimized half-open spaces into buildings and an application to a realistic case study on urban ventilation and air pollutant dispersion

Yu-Hsuan Juan [a,b], Chih-Yung Wen [c], Zhengtong Li [c], An-Shik Yang [b,d,*]

[a] Department of the Built Environment, Eindhoven University of Technology, Eindhoven, the Netherlands

[b] Department of Energy and Refrigerating Air-Conditioning Engineering, National Taipei University of Technology, Taipei, 106, Taiwan

[c] Department of Mechanical Engineering, The Hong Kong Polytechnic University, Kowloon, Hong Kong

[d] Research Center of Energy Conservation for New Generation of Residential, Commercial, and Industrial Sectors, National Taipei University of Technology, Taipei, 106, Taiwan

Abstract

The project planning activities of urban air quality and breathability have increasingly become the noticed issues around the world in recent times. In this study, the incorporation of half-open spaces into the ground corners of high-rise buildings is accomplished by slightly modifying the building morphology as a feasible solution. A unified procedure is proposed via a combined framework of parametric CFD study and multivariable regression analysis to optimize the half-open space design for improving the ventilation performance and air quality. The influences of four design parameters (i.e., the building height, width of street canyon, height and width of half-open space) are investigated. Using the results from this combined framework, CFD simulations are extended to inspect the effectiveness of merging optimized half-open space layouts into high-rise buildings as the deterministic analysis in a realistic case study. Both CFD simulations are validated with the wind tunnel data for a generic urban array and on-site measurements for realistic case study. The predictions are discussed to evaluate the outcomes of urban breathability and air pollutant dispersion by the indices of air change per hour (ACH) and purging flow rate (PFR). Integrating optimized half-open spaces into constructions can greatly affect ventilation and air pollutant at the pedestrian layer, although lesser influences on the urban canyon layer. This strategy relies on the database formulated from the CFD results of varied building morphologies in the generic urban array to realize the optimized design in a more effective and time-saving manner when applying to realistic cases.

1. Introduction

In the process of global urbanization, the high-rise buildings and high-density cities are prompt growth, causing the concerns on air pollution and associated environmental problems. The growing number of narrow streets around densely packed high-rise buildings can be the major reason for poor urban microclimate and severe air pollution in the urban canopy layer (UCL) [1]. Accordingly, good ventilation of urban areas is very important to transport cleaner airflows from the rural areas into the UCL for moderating the negative impacts of pollutants, and thereby improve the urban breathability and air quality in the entire UCL and pedestrian region [2, 3].

Recently, the good design practices of building morphology have gained importance as possible options in the beginning of design strategies to resolve the issues of urban ventilation and pollution removal in urban areas. Therefore, the optimization of building morphology to manage urban ventilation and air pollutant dispersion around buildings requires to be properly considered with the results feed backed in the decision-making process for urban development programs [4]. In this study, the implementation of half-open space into ground corners of the building is presented to well modify the building morphology as one of conceivable solutions. For the Romanesque architecture in the 10^{th}-12^{th} centuries, this distinctive building form has been called "arcade design". To better distribute and stretch the structural loads for large spans, a series of contiguous arches supported by columns or piers are built along one or both sides of the building as the half-open space (shown in Fig. 1) [5]. Arcade design can provide a sheltered walkway for pedestrians from the harsh elements and dirty streets. As a result, this building morphology has also featured in medieval cloisters, Islamic courtyards, Renaissance commercial streets and modern shopping centers. Nowadays, we are at an unprecedented time in terms of the development of high-rise buildings. However, most of the high-rise buildings need appropriately designed pedestrian shelters and fail to incorporate canopies, step-backs, or other building morphologies to create a comfortable ground-level pedestrian environment. In effects, high-rise buildings can cause windy, dark entry plazas, sidewalks and public spaces, whereas arcade buildings modify the building morphology by stepping back the massing of high-rise buildings at the ground floor toward the middle to minimize any undesirable wind impact on the outdoor space at a low height.

Previous studies show a similar building morphology modification as the open space between the ground and elevated main structures (also called the ‘lift-up’ area), which were proposed to enhance wind circulation at the pedestrian level [3, 6-9]. The present study primarily focuses on modifying less building morphology via incorporating half-open spaces into the building designs during the early stages of planning as a strategy of climatic control. Many researchers have found that the building configurations adopting half-open spaces can lead to a significant increase in local wind velocity and urban ventilation at the

pedestrian pathway layer (PPL) [9-14] and UCL [15, 16] in urban areas. Although the aforementioned research efforts suggested the use of half-open spaces to augment the ventilation performance of UCLs, most of their studies only explored the velocity patterns, without considering the pollution control. In effect, it is difficult to predict the pollutant dispersion phenomenon in an urban environment. Among various methods, computational fluid dynamics (CFD) can be promising to provide the useful information on the city breathability and air pollutant dispersion process. Two types of urban configurations were addressed in most earlier studies: generic cuboid buildings [17-19] and existing complex urban geometries [2, 20-22]. Ramponi et al. showed the studies with generic urban geometries [17]. However, the parameters, consisting of the real urban morphologies [2, 22-24], specifications of pollutant sources [19], local climatological data [25, 26] and thermal effects [27-31], should be entirely described for realistic urban areas. Meanwhile, turbulent diffusion is an important factor competing with mean flow in removing pollutants locally [32]. As a result, the CFD simulations of pollution spreading are extremely complicated in a real city. This study aims to develop the computational model for accurate predictions of pollutant dispersion in a generic urban area first, and then extend the simulations further to evaluate the effectiveness of adapted measures using the optimized half-open space design for ventilation enhancement and air pollution reduction in a realistic urban area.

High-rise buildings are common nowadays as part of most densely-populated cities, such as Hong Kong and Manhattan areas in New York. Several investigations [6, 33-35] show that the building height can substantially intensify the drag forces produced by high-rise buildings and higher pollutant dilution capacities by mean flows, but enhance turbulence characteristics in urban areas. Table 1 presents an overview of recent CFD studies focusing on the influences of aspect ratio and/or building height on the ventilation and pollutant dispersion outcomes in high-rise building layouts. The issues of urban breathability and pollution removal in street canyons have been assessed using two major types of indices, including (1) ventilation indices, such as the air change rate per hour (*ACH*) [15, 16, 29, 36] and exchange velocity [22, 33] as well as (2) pollutant indices, such as the age of air [6, 17, 32, 37], purging flow rate (*PFR*) [34], pollutant exchange rate (*PCH*) [36] and pollutant transport rates (*PTR*) [18, 34]. In this paper, both the concepts of age of air and *PFR* are implemented to evaluate pollution removal effectiveness for high-rise buildings with the arcade design. Noted that *PFR* represents the net capacity of purging ground-level pollutants by the mean flow and turbulent diffusion. Most earlier studies observe that larger street aspect ratios (*H/W*) lead to higher pollutant concentrations in street canyons [6, 16, 19, 34, 38, 39]. Accordingly, the variations of building height may affect the involvement of both mean flows and turbulent diffusion to strengthen or weaken the pollutant removal in urban areas [32]. In addition, those studies have primarily emphasized high-rise urban geometries at the street aspect ratios of street canyons less than 2 with constant or random building heights [40]. However, in a city of high-rise and high-density

buildings similar to Hong Kong, the street canyon aspect ratios are normally greater than 2, producing "wall effects" to impede the natural ventilation between building blocks [41, 42]. It is very difficult to employ the airflows above the building height to facilitate ventilation and pollutant mitigation at the pedestrian level where the buildings are tightly packed to form a narrow street. More studies are therefore needed to better understand the underlying mechanisms of pollutant dispersal and aeration in deeper street canyons at high *H/W* ratios (larger than 2). The relationship between the building configurations and pollution removal efficacy is further analyzed, Possible building solutions utilizing the half-open space design to enhance aeration and pollutant lessening at the pedestrian level are also explored.

Table 1 Overview of recent CFD studies on influences of aspect ratio and/or building height on ventilation and pollutant dispersion outcomes in high-rise building layouts

Publication	***Ref.***	***Model type***	***H/W***	***Discussion***
Chen et al. (2017)	[33]	Generic	1.5	Exchange velocity
Kubilay et al. (2017)	[19]	Generic	0.43,1, 2	Pollutant exchange velocity
Juan et al. (2017)	[15]	Realistic	3.3	*ACH*
Wen et al. (2017)	[16]	Generic	0.5~3	*ACH*
Antoniou et al. (2017)	[2]	Realistic	0.5~1	Age of air, air delay
Hang et al. (2015)	[18]	Generic	0.67~1.33	PTR, Net escape velocity (NEV)
Hang et al. (2012)	[34]	Generic	1.5~2.67	*PFR*, PTR
Hang et al. (2012)	[32]	Generic	2~4	Age of air, PTR
Hang and Li (2011)	[6]	Generic	1.5~5.3	Age of air, air exchange efficiency
Hang and Li (2010)	[39]	Generic	2~2.67	*ACH*
Hang et al. (2009)	[43]	Generic	1, 6.67	PTR
Cheng et al. (2008)	[36]	Generic	0.5, 1, 2	*ACH*, PCH
Liu et al., (2005)	[38]	Generic	0.5, 1, 2	*ACH*, PCH

Within the above context, this study aims to present the innovative application of half-open space design optimization using in high-rise buildings for sustainable urban development. In this perspective, the objectives of this work are as follows:

1) To propose and implement a combined framework for optimizing the half-open space design as the modified building morphology at the beginning of the design stage;
2) To evaluate the impact of half-open space design on urban ventilation, air quality, and pollutant removal in high-rise urban areas;
3) To quantify the capacity of urban ventilation and pollution control using the optimized half-open space layout with the uniform release of gaseous passive pollutants;

4) To present the computer-based time-saving potential of this combined framework when implementing into the realistic case study for better urban ventilation and pollutant removal.

The analysis considers isothermal turbulent airflows approaching the high-rise urban areas, and focuses on the strong channeling effect of airflow acceleration and pollutant plumes in deep street canyons with uniform pollution sources. The paper is structured as follows. In Section 2, the combined framework is described and divided into two parts: the first part is CFD parametric analysis from the generic building models in Section 2.1, while the second part is the optimal building morphology in Section 2.2. Afterwards, an application of the combined framework to a realistic scenario is shown in Section 3 to explore the effectiveness of the optimization procedures used to half-open space design for enhancing city breathability and pollution reduction. The limitations and further works are discussed in Section 4. Concluding remarks are presented in Section 5 for using the half-open space design to realize attractive well-designed buildings and sustainable urban environments.

2. Description of the combined framework

The combined framework and how it applies to target buildings is depicted in Fig. 2 as two parts. For the first part - before the design stage, it consists of two main steps:

- Step1 – Database of CFD results obtained from the generic building models: A set of parametric analysis for the modified building morphology in the generic urban array is conducted by CFD simulations to attain the ventilation outcomes (Section 2.1).
- Step 2 – A multivariable regression analysis: Investigation among the parametric factors can resolve the correlation between ventilation outcomes and design parameters (Section 2.2).

For the second part - at the beginning of the design stage, it presents an application of using the above correlations to optimize the half-open space design in a realistic case study (Section 3).

2.1. CFD parametric analysis for a generic building array

2.1.1. Generic model description and simulation setup

The present parametric analysis investigates the urban ventilation performance for four ideal full-scale building blocks in a 7 × 11 array with a medium density (a building packing density $\lambda p = 0.25$). There are 17 test cases studied to elucidate the influences of the following four parameters of the half-open space in ideal street canyons, as shown in Fig. 3:

- The building height (H): H varies from 15 m to 90 m.
- The width of street canyon (W): W varies from 15 m to 90 m.
- The height of the half-open space (h): h varies from 1.5 m to 9 m.

- The width of the half-open space (w): w varies from 1.5 m to 9 m.

The 3D building array with the characteristic dimensions of building width B = building length L = 30 m with the ratio of H/W varying from 0.33 to 3. This analysis investigates the effects of street canyon type and half-open space morphology on the aeration of urban climate. Figure 4(a) displays one of the cases representing a conventional high density area with H/W= 3 with a typical half-open space of 3 m high (h) and 3 m wide (w). Many traditional half-open spaces have a 3-m height on the ground floor in the regions with hot and humid climates such as Japan, China, Malaysia and Taiwan [15]. Figure 4(b) shows the computational domain setup. The distances from the urban boundaries to the top, inlet, outlet and lateral boundaries are 6H, 5H, 20H and 6H, respectively, to avoid the occurrence of unwanted stream wise gradients as well as allow the complete development of a wake region behind the buildings, facilitating the convergence of simulations. In the wall functions, the wall roughness is expressed through an equivalent sand-grain roughness k_S, corresponding to 30 times that of z_0 [43]. In calculations, the arrangements of the domain extent, grid size and boundary conditions are in compliance with the requirements of the CFD guidelines [44, 45]. We employ the hexahedral cells with a grid expansion ratio of 1.2 to resolve the rapid variations of flow properties associated with the interaction of the wind with buildings, as depicted in Fig.5. To layout the numerical mesh, only hexahedral cells are implemented to realize the smallest cell volume of around 2.7×10^{-2} m^3 adjacent to the ground and building walls. A total number of 29,108,169 points is used to construct the mesh setup for a building morphology with half-open space.

To explore the wind environments adjacent to the subject building with half-open spaces, we perform numerical computations employing the ANSYS/Fluent® software (Release 18.0) to simulate the flow of terrestrial wind over ideal urban street canyons with half-open space designs for evaluating the ventilation and pollution dispersion outcomes over urban canyons. The theoretical analysis is based on the steady-state 3D conservation equations of mass and momentum for incompressible isothermal turbulent flow. More details related to the equations can be found in Ref. [17, 44, 45]. The Reynolds-averaged Navier-Stokes (RANS) turbulence modeling is applied to estimate the ventilation (in terms of the airflow velocities and turbulent kinetic energy) in the UCL. These four turbulent models are later verified by the wind tunnel measurements. We adopt the atmospheric boundary layer (ABL) flow as the inlet boundary condition to model the related atmospheric processes. Table 2 shows all details of boundary conditions.

Table 2 Boundary conditions of CFD simulations

Boundary conditions	***Type***	***Details***

Inlet	Velocity-inlet	$U(z) = 3.0 \times (z/H)^{0.16}$ $k(z) = \frac{(u^*)^2}{\sqrt{C_\mu}}$ $\varepsilon(z) = C_\mu^{3/4} k^{3/2} (K_v z)$ where H, u^* and K denote the building height, friction velocity (0.24 m/s) and the von Karman's constant (≈ 0.4). A full-scale aerodynamic roughness length of z_0 = 0.1 m. Reynolds number of ~30,000, as in the expereiment [40]
Outlet	Pressure-outlet	Constant static gauge pressure (1 atm)
Top	Symmetry	
Lateral		
Building	Wall	No slip boundary condition with a standard wall function
Ground		

2.1.2. Design objectives and variables

To evaluate the influence of half-open space design on the urban ventilation, the *ACH* is considered as one of imperative factors defined by the volumetric air exchange rate (Q_{in}) of the complete pedestrian pathway layer (PPL) from the ground to a height of 3 m for assessing the ventilation outcomes. The term Q_{in} is computed by integrating over the whole street canyon. The *ACH* can be expressed as below.

$$ACH = 3600 \frac{Q_{in}}{Vol}. \quad (2)$$

The *ACH* has a unit of h^{-1} and *Vol* is the PPL volume (m^3). The *ACH** (defined as the ratio of the *ACH* to a characteristic frequency, calculated by the reference velocity of the far upstream free flow divided by the reference building height) results of the correlations derived from the multivariable regressions based on generic urban street canyons as the guidelines.

To investigate the urban air quality, this study adopts the concept of local mean age of air to appraise the freshness of air within the building canyons and purification of urban air environments by the rural fresh air simultaneously. Considering the pollutant sources released with a certain initial concentration, attenuation of the concentration can be conceived as the travel of the pollutants within the incoming wind flow and mixing with clean air. To evaluate

the pollutant spreading, a homogeneous emission rate to calculate the local mean age of air τ (in s) is used and defined as below.

$$\tau = \frac{c}{S_c}, \tag{3}$$

where c denotes the pollutant concentration (kg/m^3) with S_c of 10^{-7} kg/m^3-s as the reference concentration. In essence, a uniform emission rate S_c is assumed within the UCL space. As a result, the local concentration can stand for how much pollutant transfers out of the initial pollutant set up region in Fig. 3.

In analyzing pollution dispersion, both the flow field and source arrangements (locations and release strength) can significantly influence pollutant concentration. Therefore, the setting of pollutant sources is important to quantify and compare the ventilation capacity outcomes of removing pollutants for different scenarios. In a zone where a passive contaminant source is formed with uniform release strength, the purging flow rate (m^3/s) is the net flow rate by which the pollutants are purged out of the zone [46]. As the most crucial index for defining the ventilation efficiency, *PFR* indicates the capacity of the wind in removing the pollutants from the objective domain. To appraise the net capacity of removing pedestrian pollutants by both mean flow and turbulent diffusion, the pedestrian *PFR* is described as [40]:

$$PFR = \frac{S_c \times Vol}{C} \tag{4}$$

Here the sign C is the spatially averaged concentration in the entire PPL volume (*Vol*). Many studies have used this concept for assessment of pollution control in the urban environments [40, 47].

2.1.3. CFD validation for a generic building array

This study first replicates the extent of wind tunnel and geometrical details of test objects from the experimental setup to generate a 3D building array model for validation purposes in Fig.6 [40]. In the wind-tunnel experiments by Brown et al. [48], the measurements were made in the open return wind tunnel of the Fluid Modeling Facility in the US Environmental Protection Agency. A generic urban configuration includes the arrays of cubic building blocks (seven rows of eleven columns) with the characteristic dimensions of height (H_{wt}) = width (W_{wt}) = length (L_{wt}) = 0.15 m. For this urban configuration, the frontal area density (λ_f, the ratio of the frontal area of buildings to the total floor area) and the building area density (λ_p, the ratio between the planar area of

buildings viewed from above and the total floor area) are 0.25 and 0.25, respectively, while the *H/W* is 1. The scale ratio between wind tunnel models and full-scale cubic building arrays is 1:200. The full-scale cubic building arrays are therefore numerically investigated with *H*= *W*= *L*= 30 m. The dimensions of computational domain are disposed using the best practice guidelines [49, 50]. In this case, the upstream, downstream and top length of the domain are 5H, 19.2H and 6H, respectively, with 8H set as the lateral length of the domain. The grid setup only involves the hexahedral cells with a total number of 24,076,524 points. We arrange 15 cells over the width of street canyons to better resolve the associated flow velocity across the street. Those cells in the nearby surroundings of buildings implement a maximum stretching ratio of 1.1 with the smallest and greatest cell volumes of around 1×10^{-6} m^3 and 9.2×10^{-5} m^3, corresponding to the y^+ values of 30 to 350. These values can locate the wall-adjacent cells in the logarithmic layer to well comply the requirements of using the standard wall functions. The grid is based on a grid-sensitivity analysis. ABL and other details of boundary conditions are illustrated in Table 2.

We also conduct a sensitivity study of four widespread turbulence models, specifically, the standard *k-ε*, realizable *k-ε*, RNG *k-ε* and SST *k-ω* turbulence models. The predictions from four turbulent models are verified by the wind tunnel measurements. Fig. 6 illustrates a comparison of the predictions using the standard, realizable, RNG *k-ε* and SST *k-ω* models with the measurements of X velocity, Z velocity and turbulence kinetic energy in the middle of the initial street canyon at x/H= 1.5 for CFD validation. We observe that the calculated X velocity and turbulent kinetic energy profiles from the standard and realizable *k-ε* models are relatively more accurate than those from the RNG and SST *k-ω* models. Furthermore, the simulated results of the Z velocity profiles with the standard and RNG *k-ε* models agree reasonably well with the measured data. Hence, the prediction capability of the standard *k-ε* turbulence model reveals the best outcomes of optimal agreement of the CFD predictions with wind tunnel measurements than those from the realizable, RNG *k-ε* and SST *k-ω* models.

2.1.4. Database of CFD results

The CFD parametric analysis is conducted to quantify the ventilation in the UCL and PPL for exploring the effects of integrating half-open spaces into buildings on the related aeration performance in terms of the *ACH* results. Here the UCL is defined as the air volume from the ground to the building height. In addition, the PPL is denoted as the space lower than a height of 3 m above the ground. The effects of modified building morphology can notably affect the ventilation in PPL than that in the entire UCL, due to the presence of half-open spaces. The results show that the half-open space design can achieve much better ventilation outcomes in the PPL than UCL due to the deployment of half-open space near the ground. Table 3 shows the ventilation results of ACH* in PPL for the parametric analysis of different modified half-open space designs. For four important variables, it has been found that 16 simulated conditions

would be a thorough factorial experiment [51]. It requires fewer experimental subjects but still keeps the ability to investigate the interactions between factors. Thus, this parametric analysis conducts CFD simulations using 16 scenarios with four parameters of half-open space as a useful strategy by applying the Design of experiments (DOE) for Step 2 of the combined framework. The strategically planned and executed simulations can provide useful information on the relationship of the urban ventilation performance with a response variable due to the variations of one or more factors in the modified building morphology.

Table 3 CFD results of parametric analysis on ventilation performance of various half-open space layouts in generic high-rise urban areas

Case name	*Predicted independent variables*				*Responsively dependent variable*
	H (m)	W (m)	h (m)	w (m)	ACH*
1	30	30	3	3	170.41
2	15	30	3	3	118.92
3	22.5	30	3	3	169.15
4	45	30	3	3	185.84
5	60	30	3	3	195.84
6	90	30	3	3	232.43
7	30	15	3	3	275.08
8	30	40	3	3	145.90
9	30	60	3	3	119.51
10	30	90	3	3	90.79
11	30	30	4.5	3	130.38
12	30	30	5	3	130.13
13	30	30	6	3	128.44
14	30	30	3	9	253.74
15	30	30	3	6	210.23
16	30	30	3	4.5	187.92
17	30	30	3	1.5	148.69

2.2. Optimal building morphology

2.2.1. Multivariable regression analysis

Multivariate regression analysis (MRA) is a method utilized to develop a linearly related correlation between the predicted independent variables and responsively dependent variables. This study can accurately predict the behavior of responsive variable of *ACH* associated with the changes in modified parameters of building morphology. Based

on the CFD predictions of the above parametric analysis, a second-order correlation has been established with the sum of $R^2 = 0.97$, as given in our previous study [16]:

$$\frac{ACH}{U_{ref}/z} = 52.1506 + 6.64139\left(\frac{H}{W}\right)^2 + 64.3169\left(\frac{h}{w}\right)^2 - 3.34449\left(\frac{H}{h}\right)^2 - 107.435\frac{H}{W}$$

$$-13.2081\frac{h}{w} + 37.0701\frac{H}{h} - 120.478\frac{H}{W}\frac{h}{w} + 31.8608\frac{H}{W}\frac{H}{h} - 7.32217\frac{h}{w}\frac{H}{h}. \quad (5)$$

Here ACH is normalized utilizing the characteristic frequency U_{ref}/z. According to Eq.(5), the building morphology optimization of half-open spaces with multiple parameters can serve as a useful reference for future object buildings at the beginning of the design stage.

2.2.2. Optimal design of building morphology from MRA

To attain the optimal design of building morphology, a generic high-rise buildings array (B= W= 30 m) with the identical average height (H= 90 m) is used as the most representative high-rise urban layout. Although limited to the simple airflow problems, this layout can still provide a suitable estimate for urban planning uses as well as an analytical model to achieve a better understanding of the urban physics. The optimal half-open space design of the factors *h* and *w* can be then elucidated by Eq.(5) of MRA with inputted *H* and *W* to reflect the above urban morphology. An apparent ascending trend shows that *ACH* increased with *w* at *h*= 4 m, suggesting better ventilation performance realized with a wide arcade in buildings. In view of the limitation of the reasonable building width, the highest amount of ventilation is acquired at the maximum arcade width of 9 m, indicating the fine selection of the optimized half-open space configuration of 4 m high and 9 m wide.

2.2.3. Verification of MRA results in ideal urban morphology

CFD simulations are conducted to compare the urban ventilation outcomes of optimized half-open space layout (Case 2) by MRA with those of typical half-open space layouts (Case 1) for the comparison purpose. In practice, a typical half-open space layout has 3 m high and 3 m wide. Figure 7 presents the predicted velocity magnitude contours and streamlines in (a) the vertical cross-sectional plane of Y= 0 m and (b) the horizontal cross-sectional plane at a pedestrian height of Z = 1.75 m for the typical (Case 1) and optimized (Case 2) half-open spaces. To observe the mean flow patterns in the presence of half-open spaces, there is a fully developed region starting at a certain distance from the windward entrance. In Fig. 7(a), one part of incoming wind passes over the street roof upwardly, while another part of wind runs into

the entire street canyons. Although the presence of windward walls tends to channel air flowing upwardly and thereby diminish the amount of air entering into the windward entries, high-rise buildings essentially block the approaching wind with high pressures generated at windward walls and direct a part of air into the entries laterally, indicating considerable air flow rates across the windward entries. As the incoming wind diverges from the first building, it is also observed that a substantial amount of fresh air streams downward in the front of the first building, and then enters into street canyons. Elevated velocities appeared near the lateral sides of buildings owing to local flow acceleration induced from the corner expansion effect. For the typical arcade layout (Case 1), Fig. 7(b) shows a large recirculating vortex on the leeward side of first-row buildings, and a pair of small vortices resides over an essentially low-speed region behind second-row buildings. In contrast, the optimized arcade layout for Case 2 leads to relatively higher wake flow velocities without the presence of vortex eddies around the back of the first-row buildings. The vortex eddies around the second-row buildings for Case 2 is also more diffusive and weaker.

Table 4 presents a comparison of the *ACH** estimated by the correlation from MRA with CFD predictions for the typical (Case 1) and optimized (Case 2) half-open space layouts. Based on the same configuration of urban street canyon (*H/W*= 3), the predicted *ACH** values using Eq. (5) from the MRA are 229.162 and 854.127 for the typical and optimized half-open space layouts, respectively. As seen, the *ACH** value for Case 2 is much greater than that of the design in Case 1. Meanwhile, the CFD predictions of *ACH** for the typical and optimized half-open space layouts are 362.833 and 926.552, indicating the effectiveness of utilizing the correlation from MRA as an building morphology optimization guideline to determine the optimal half-open space design of *h*= 4 m and *w*= 9 m for enhancement of urban ventilation in conventional high density urban areas (*H/W*= 3). The CFD predictions provide a 155% higher *ACH** value in Case 2 than that in Case 1.

Table 4 Comparison of *ACH** computed by correlation from MRA with CFD predictions for typical and optimized half-open space layouts

Case name		Half-open space layout		*ACH**	
		Height *h* (m)	Width *w* (m)	Eq.5 from MRA	CFD Results
Typical	Case 1	3	3	229.162	362.833
Optimized	Case 2	4	9	854.127	926.552

3. Application of combined framework to realistic case study

3.1. Geometry setup of case study

To investigate the effectiveness of utilizing half-open space design into buildings as the control measures on the reduction of atmospheric particulate pollution in realistic high-rise urban areas, the studied site primarily includes a crossroad enveloped by several typical high-rise buildings in the Sanxia District, located at latitude 24°9'N (121°37'E), in the hub of central New Taipei City, Taiwan, as presented in Fig. 8. The complicated high-rise and high-density urban area is composed of low-high-rise buildings with an approximately average height of 90 m. The area of interest involves narrow streets with the widths varying from 27 m to 33 m. Most of the buildings under study have typical half-open space designs, which are suitable to explore city breathability and pollution mitigation in this densely urbanized area. The present scenario considers a conventional UCL parameter of H/W= 3.33 in realistic high-density areas. CFD simulations are conducted using the original half-open space design with 4.5 m high and 3 m wide in Cases R1. For the optimized half-open space layout of Case R2, as given in Section. 2.2, we apply the optimization procedures of MRA to adopt the optimal half-open space design of h= 4 m and w= 7.5 m for maximizing the ventilation outcome at the highest ACH* value. Accordingly, this study implements the optimal half-open space design to inspect its effectiveness of pollution removal in realistic high-rise urban areas.

This section probes the pollution dispersal outcomes of the subject crossroad surrounded by the buildings having the typical and optimized half-open space layouts in realistic high-rise urban areas (*H/W*=3.33). Figure 9 shows the study site with the geometric extents of 1740 m long, 1050 m wide and 90 m high, respectively. The overall computational domain is 12000m× 19500 m× 600 m (length× width× height). The upstream domain length is kept as short as possible to circumvent the occurrence of unintended streamwise gradients. Furthermore, the downstream domain length is long enough to allow the full development of the wake region behind the structures, which can facilitate the convergence of iterations during simulations.

In the simulations of complex realistic high-rise urban, the mesh system consists of finer hexahedral cells around the regions neighboring the crossroad of the four objective high-rise buildings and near the boundary surfaces of half-open space, with an averaged cell volume of around 8×10^{-3} m^3. Other parts of the numerical mesh utilize a hybrid grid approach of tetrahedral and hexes around the building geometries and boundaries with a grid expansion ratio of 1.2. The average cell volumes are 1 m^3 with the smallest cell volume of 2.7×10^{-2} m^3. Regarding the grid independence check, three calculations are conducted with total grid numbers of 33,855,588, 42,045,462 and 67,254,195, respectively. The satisfactory grid independence is attained using the medium grid with 42,045,462 cells, having the greatest velocity magnitude difference of 1.36% compared with the case of 67,254,195 cells.

3.2. Computational settings and parameters

In CFD simulations, this study implements the realizable k-ε turbulence model, which is based the pedestrian-level wind conditions in our earlier successful validation studies verified by on-site measurement data [15]. In practice, we adopt the average reference speed of 10.07 m/s at a reference building height of 92.5 m from the northeast of the studied site during the summer (from June to August) over the past ten years. In addition, the weather data from the meteorological station are employed as the inflow boundary conditions to calculate the neutral ABL velocity profile as follows:

$$U_{ABL} = \frac{u^*_{ABL}}{K} \ln\left(\frac{z + z_0}{z_0}\right), \tag{6}$$

The ABL friction velocity u^*_{ABL} can be computed from a specified velocity U_h at a reference height h.

$$u^*_{ABL} = \frac{KU_h}{\ln\left(\frac{h + z_0}{z_0}\right)}. \tag{7}$$

This study utilizes the wall function setup in CFD to model the effect of real obstacles on the wind with the wall roughness parameters to simulate the drag (from those barriers) applied to the ground surfaces, which is expressed adopting an equivalent sand-grain roughness k_S in the wall functions [52]. The mean air temperature of typical summer days in the Sanxia District is 29.5°C. The corresponding values of the density, viscosity and conductivity are 1.163 kg/m^3, 1.869×10^{-5} N-s/m^2 and 2.639×10^{-2} W/m-k. To describe the urban area of the studied site, the aerodynamic roughness z_0 is set greater than 2 m, based on the updated Davenport roughness classification for the city center forms, which are composed of low-high-rise buildings in a high-rise and high-density urban area [53].

In the CFD simulations to assess the urban air quality, the pollutants released by vehicles are assumed to be well mixed at the height from 0 to 2 m above the ground owing to vehicle motions, as depicted in Fig. 3. This method of simplification is consistent with previous studies [18, 34, 43], prescribing uniform passive volume pollutant sources (CO) to simulate the perfectly-mixed near-ground pollutant emissions rate of $S_c = 10^{-7}$ kg/m^3-s. It also considers the insignificant disturbances of released emission to the wind flow in all scenarios. The CFD simulations first determine the turbulent airflow field, and then solve the steady- state species transport equation to acquire the pollutant concentration distribution (c) [40]:

$$u_j \frac{\partial c}{\partial x_j} - \frac{\partial}{\partial x_j}\left(D_t \frac{\partial c}{\partial x_j}\right) = S_C, \tag{8}$$

here the sign u_j is the velocity component in the j axis, and D_t is the turbulent diffusivity of pollutants, defined as $D_t = \nu_t/S_{ct}$. The symbol ν_t is the turbulent viscosity, whereas S_{ct} is the turbulent Schmidt number, showing the ratio of momentum diffusivity to pollutant diffusivity. Though S_{ct} varies with different gradients of pollutant concentration and flow structures, S_{ct} is usually treated as a constant ranging from 0.2 to 1.3 to compensate the under-estimation of the turbulent mass diffusion by the RANS models [17, 54-58]. According to Refs. [19, 58], a value of $S_{ct} = 0.7$ is specified as the standard value to perform CFD simulations for all cases. To set the boundary conditions, we prescribe the inflow pollutant concentration at the inlet to be nil, and impose zero normal gradients of pollutant concentration on the roof, outlet and all wall surfaces. Generally, each solution procedure is found to take approximately 120 hours of CPU time to achieve a converged solution executed on an Intel® Xeon® E5-2670 v3-2.3 GHz (×2 processors, 192 GB RAM) high-performance workstation. Besides, the description on the validation study in realistic high-rise urban areas is given in a separate paper [15].

3.3. CFD validation for a realistic case study

The on-site measurements were conducted for the CFD validation of the target building model of high-rise urban environments in our prior study [15] Three sets of Testo 480 climate instruments with thermal flow velocity probes (Testo 0635 1050) covered 15 monitoring points to measure the airflow velocities during daytime at hourly basis from 10:00 to 18:00h over 7 days from July 28 to August 3, 2015. The predicted velocities were distributed around the periphery of the crossroad and in the middle of street canyons surrounded by those main high-rise buildings at a height of 1.5 m, except for the reference point at 92.5 m above the ground. To validate the accuracy of the predicted flow field of realistic high-rise urban areas, Fig. 10 presents a comparison of the CFD predictions of velocity magnitude from the standard, realizable and RNG k–ε models, respectively, with the on-site measurement data. It is seen that all the predictions by the realizable k–ε model are in the range of the error bars designated by ±3 standard deviations, while the standard and RNG k-ε models significantly overpredict the velocity magnitude values for half of the measured points. Thus, the realizable k–ε model has greater consistencies with the measured data, as compared to the standard and RNG k–ε models.

3.4. CFD results for a realistic high-rise urban areas

To quantitatively describe the flow patterns of the wind over the realistic high-rise urban area, Fig. 11(a) illustrates the predicted contours of velocity magnitude in the horizontal cross-sectional plane at a pedestrian height of Z= 1.75 m for the original (Case R1) and optimized (Case R2) half-open space layouts. For the latter, the predictions demonstrate a substantial increase in the wind velocity from 0.3 to 4.5 m/s due to the optimization of half-open spaces. It is clearly observed that the optimized half-open space design tends to induce higher airflow

velocities over the center of the crossroad and the wake region, as compared to the original half-open space layout. In Case R2, the wind blows through the urban canyon of high-rise buildings, and thus produces stronger ventilated flows over the crossroad than those in Case R1. Besides, an original half-open space layout in Case R1 reveals a relatively lower increase in the wind velocity from 0.1 to 3.6 m/s around the crossroad region due to reduced airflow rates across the half-open space openings. Figure 11(b) presents the predicted contours of the local mean age of air in a horizontal cross-sectional plane at a pedestrian height of Z= 1.75 m for the original and optimized half-open space layouts. The predictions in Case R2 evidently revealed a lower local mean age of air distribution in the crossroad region as compared to that in Case R1 owing to more airflow rates induced by the optimized half-open space layout to flush the main street and crossroad for pollutant attenuation at the pedestrian level. In Case R1, higher values of the local mean age of air appear on the leeward side of crossroad region, with the associated value of around 30~56 s. However, utilizing the optimize half-open space layout (Case R2), the predictions indicate the lower local mean age of air values of approximately 22~45 s on the leeward side transported further downstream.

Figure 12 exhibits the computed ACH* and PFR outcomes for the original and optimized half-open space layouts. For an optimized half-open space design (Case R2), the ACH* is considerably augmented as a result of more fresh airflows transported into PPL from a wider half-open space layout, indicating the best ventilation performance at a peak value of 816.97 with a 75% higher ACH* value than that of the original half-open space design (Case R1). In addition, the predictions reveal similar tendencies with better aeration and PFR outcomes of pollution removal for the half-open space designs. For the optimized half-open space layout, PFR value of 5468.774 m3/s is 57% higher than that of the original half-open space design (Case R1). Hence, the predictions manifestly suggest the substantial improvements of ACH* and PFR in PPL, confirming the effectiveness of achieving better pedestrian ventilation and pollution removal by the optimized half-open space, similar to the results for the idealized high-rise urban areas described in Section 2.1.3. The calculated PFR in PPL is also essentially augmented by increasing the air change rate per hour for enhancement of city breathability.

4. Discussion

The limitations of this study are given as follows and will be addressed in future work.

(1) CFD simulations of the realistic case study primarily consider the steady incompressible isothermal turbulent flow over the high-rise urban area for an average summer condition, designating the negligibly temporal fluctuations in wind velocity, direction and diurnal temperature amplitude. Besides, the effects of solar radiation on street canyon ventilation are insignificant under the isothermal condition.

(2) Attributable to the high computational cost and complexity for particular problems, CFD simulations of the realistic case study are conducted by the most probable wind condition in the study site, with the flow from the northeast as only one wind direction of boundary conditions for an average summer day in realistic high-rise urban areas.

(3) CFD validation of this paper are based on prior studies [15, 16], reporting the verification results of the same numerical models for the velocity magnitude and turbulence kinetic energy in both case studies of generic and realistic building models. Further researches necessitate the experimental data of pollutant concentration distribution for the validation studies to predict the pollution dispersion with better accuracy in an urban environment.

(4) This study uses the *ACH* and *PFR* estimates as the effective ventilation and pollution spreading indicators to determine the performance of the city breathability and pollutant removal effectiveness. Future works can employ and compare more different ventilation and pollutant indexes.

In spite of the aforementioned limitations, the issue of concern here is on optimizing the building morphology design to improve the urban microclimate. The combined framework confirms that the optimized half-open space as modified building morphology based on CFD simulations and MRA can effectively enhance the ventilation and air quality on the realistic case study at the beginning of the design stage.

5. Conclusions

This study presents an efficient procedure to attain the optimized half-open space design of modified building morphology for improving the ventilation performance and air quality in the urban areas. The procedure is built via a combined framework of a set of CFD parametric simulation and multivariable regression analysis. Employing the results from this combined framework, the aerodynamics of various building morphologies can be identified at different urban layouts to realize good outcomes of city breathability and pollution reduction. Having the proposed procedure utilized in a case study for a realistic high-rise area, CFD simulations are performed as the deterministic analysis, and the obtained results are discussed to evaluate the ventilation and pollution dispersal of varied half-open space configurations. The simulated results for each stage are demonstrated to be consistent and are easily followed until reaching an optimized half-open space arrangement. ACH* and PFR are then applied as useful indices to quantify the ventilation and pollutant removal capacities in PPL for different half-open space layouts. For the verification of MRA results in ideal urban morphology, the estimated ACH* value of the optimal half-open space design is much greater than that of the typical one in common idealized high-rise urban areas. It is also found that the vortex region in street canyons for the optimal half-open space layout is noticeable smaller than that in the typical case, suggesting reduced pollutant accumulation in the recirculating eddies for the optimized half-open space layout. For the application of the combined framework to the realistic case study,

the effectiveness of the proposed procedure has proved the effects of optimal half-open space on the enhancement of city breathability and pollution elimination in the realistic high-rise urban areas. The present procedure of building morphology optimization is suitably implemented in similar studies to facilitate the implementation of building design or urban planning projects at the beginning of the design stage for sustainable development.

Acknowledgment

This study represents part of the results obtained under the support of Ministry of Science and Technology, Taiwan, ROC (Contract No.: MOST109-2221-E-027-011-MY2 and 107-2917-I-027-001) and Environment and Conservation Fund, Hong Kong, ECF 51/2016.

Nomenclature

ACH	= Air change rate per hour
ACH^*	= Normalized air change rate per hour
C	= Averaged pollutant concentration
C_μ,	= Turbulent constant, 0.09
$C_{\varepsilon 1}$,	= Turbulent constant, 1.44
$C_{\varepsilon 2}$	= Turbulent constant, 1.92
g_i	= Gravitational acceleration in the i axis
H	= Height of street canyon/building
H/W	= Street aspect ratio
I	= Average turbulence intensity
K	= von Kármán constant, 0.42
k	= Turbulent kinetic energy
L	= Turbulence length scale
P	= Turbulent production term
p	= Pressure
S_c	= Emission rate
u^*	= Friction velocity
u^*_{ABL}	= ABL friction velocity
u_i	= Velocity component in the i axis
U_{ABL}	= Mean inlet velocity of atmospheric boundary layer
x, y, z	= Coordinates
W	= Width of street canyon
Z_0	= Roughness length
β	= Thermal expansion coefficient
ε	= Turbulent energy dissipation rate
ε_{ext}	= Air emissivity of external field, 0.05
μ	= Dynamic viscosity
μ_t	= Turbulent viscosity
μ_{eff}	= Effective viscosity
ρ	= Density of the fluid
τ	= Age of air
τ_{ij}	= Deviatoric stress tensor

σ_k = Turbulent constant, 1.0

σ_ε = Turbulent constant, 1.3

References

[1] Hang J, Luo Z, Wang X, He L, Wang B, Zhu W. The influence of street layouts and viaduct settings on daily carbon monoxide exposure and intake fraction in idealized urban canyons. Environmental Pollution. 2017;220, Part A:72-86.

[2] Antoniou N, Montazeri H, Wigo H, Neophytou MKA, Blocken B, Sandberg M. CFD and wind-tunnel analysis of outdoor ventilation in a real compact heterogeneous urban area: Evaluation using "air delay". Building and Environment. 2017;126:355-72.

[3] Mittal H, Sharma A, Gairola A. A review on the study of urban wind at the pedestrian level around buildings. Journal of Building Engineering. 2018;18:154-63.

[4] Yu Y, Kwok KCS, Liu XP, Zhang Y. Air pollutant dispersion around high-rise buildings under different angles of wind incidence. Journal of Wind Engineering and Industrial Aerodynamics. 2017;167:51-61.

[5] Dincyurek O, H. Mallick F, Numan I. Cultural and environmental values in the arcaded Mesaorian houses of Cyprus. Building and Environment. 2003;38:1463-73.

[6] Hang J, Li Y. Age of air and air exchange efficiency in high-rise urban areas and its link to pollutant dilution. Atmospheric Environment. 2011;45:5572-85.

[7] Du Y, Mak CM, Li Y. Application of a multi-variable optimization method to determine lift-up design for optimum wind comfort. Building and Environment. 2018.

[8] Weerasuriya AU, Zhang X, Lu B, Tse KT, Liu C-H. Optimizing Lift-up Design to Maximize Pedestrian Wind and Thermal Comfort in 'Hot-Calm' and 'Cold-Windy' Climates. Sustainable Cities and Society. 2020;58:102146.

[9] Zhang X, Tse KT, Weerasuriya AU, Kwok KCS, Niu J, Lin Z, et al. Pedestrian-level wind conditions in the space underneath lift-up buildings. Journal of Wind Engineering and Industrial Aerodynamics. 2018;179:58-69.

[10] Kim T, Kim K, Kim BS. A wind tunnel experiment and CFD analysis on airflow performance of enclosed-arcade markets in Korea. Building and Environment. 2010;45:1329-38.

[11] Hang J, Luo Z, Sandberg M, Gong J. Natural ventilation assessment in typical open and semi-open urban environments under various wind directions. Building and Environment. 2013;70:318-33.

[12] Carrilho da Graça G, Martins NR, Horta CS. Thermal and airflow simulation of a naturally ventilated shopping mall. Energy and Buildings. 2012;50:177-88.

[13] Kato S, Murakami S, Takahashi T, Gyobu T. Chained analysis of wind tunnel test and CFD on cross ventilation of large-scale market building. Journal of Wind Engineering and Industrial Aerodynamics. 1997;67–68:573-87.

[14] Ai ZT, Mak CM. A study of interunit dispersion around multistory buildings with single-sided ventilation under different wind directions. Atmospheric Environment. 2014;88:1-13.

[15] Juan Y-H, Yang A-S, Wen C-Y, Lee Y-T, Wang P-C. Optimization procedures for enhancement of city breathability using arcade design in a realistic high-rise urban area. Building and Environment. 2017;121:247-61.

[16] Wen C-Y, Juan Y-H, Yang A-S. Enhancement of city breathability with half open spaces in ideal urban street canyons. Building and Environment. 2017;112:322-36.

[17] Ramponi R, Blocken B, de Coo LB, Janssen WD. CFD simulation of outdoor ventilation of generic urban configurations with different urban densities and equal and unequal street widths. Building and Environment. 2015;92:152-66.

[18] Hang J, Wang Q, Chen X, Sandberg M, Zhu W, Buccolieri R, et al. City breathability in medium density urban-like geometries evaluated through the pollutant transport rate and the net escape velocity. Building and Environment. 2015;94:166-82.

[19] Kubilay A, Neophytou MKA, Matsentides S, Loizou M, Carmeliet J. The pollutant removal capacity of urban street canyons as quantified by the pollutant exchange velocity. Urban Climate. 2017;21:136-53.

[20] Toparlar Y, Blocken B, Vos P, van Heijst GJF, Janssen WD, van Hooff T, et al. CFD simulation and validation of urban microclimate: A case study for Bergpolder Zuid, Rotterdam. Building and Environment. 2015;83:79-90.

[21] van Hooff T, Blocken B. Coupled urban wind flow and indoor natural ventilation modelling on a high-resolution grid: A case study for the Amsterdam ArenA stadium. Environmental Modelling & Software. 2010;25:51-65.

[22] Panagiotou I, Neophytou MKA, Hamlyn D, Britter RE. City breathability as quantified by the exchange velocity and its spatial variation in real inhomogeneous urban geometries: An

example from central London urban area. Science of The Total Environment. 2013;442:466-77.

[23] Mons V, Margheri L, Chassaing JC, Sagaut P. Data assimilation-based reconstruction of urban pollutant release characteristics. Journal of Wind Engineering and Industrial Aerodynamics. 2017;169:232-50.

[24] Ricci A, Kalkman I, Blocken B, Burlando M, Freda A, Repetto MP. Local-scale forcing effects on wind flows in an urban environment: Impact of geometrical simplifications. Journal of Wind Engineering and Industrial Aerodynamics. 2017;170:238-55.

[25] Yang AS, Juan YH, Wen CY, Su YM, Wu YC. Investigation on Wind Environments of Surrounding Open Spaces Around a Public Building. Journal of Mechanics. 2017;33:101-13.

[26] Yang A-S, Su Y-M, Wen C-Y, Juan Y-H, Wang W-S, Cheng C-H. Estimation of wind power generation in dense urban area. Applied Energy. 2016;171:213-30.

[27] Cui P-Y, Li Z, Tao W-Q. Buoyancy flows and pollutant dispersion through different scale urban areas: CFD simulations and wind-tunnel measurements. Building and Environment. 2016;104:76-91.

[28] Allegrini J, Carmeliet J. Coupled CFD and building energy simulations for studying the impacts of building height topology and buoyancy on local urban microclimates. Urban Climate. 2017;21:278-305.

[29] Yang A-S, Wen C-Y, Juan Y-H, Su Y-M, Wu J-H. Using the central ventilation shaft design within public buildings for natural aeration enhancement. Applied Thermal Engineering. 2014;70:219-30.

[30] Yang A-S, Juan Y-H, Wen C-Y, Chang C-J. Numerical simulation of cooling effect of vegetation enhancement in a subtropical urban park. Applied Energy. 2017;192:178-200.

[31] Mirzaei PA, Haghighat F. A procedure to quantify the impact of mitigation techniques on the urban ventilation. Building and Environment. 2012;47:410-20.

[32] Hang J, Li Y, Buccolieri R, Sandberg M, Di Sabatino S. On the contribution of mean flow and turbulence to city breathability: The case of long streets with tall buildings. Science of The Total Environment. 2012;416:362-73.

[33] Chen L, Hang J, Sandberg M, Claesson L, Di Sabatino S, Wigo H. The impacts of building height variations and building packing densities on flow adjustment and city breathability in idealized urban models. Building and Environment. 2017;118:344-61.

[34] Hang J, Li Y, Sandberg M, Buccolieri R, Di Sabatino S. The influence of building height variability on pollutant dispersion and pedestrian ventilation in idealized high-rise urban areas. Building and Environment. 2012;56:346-60.

[35] Ai ZT, Mak CM. CFD simulation of flow in a long street canyon under a perpendicular wind direction: Evaluation of three computational settings. Building and Environment. 2017;114:293-306.

[36] Cheng WC, Liu C-H, Leung DYC. Computational formulation for the evaluation of street canyon ventilation and pollutant removal performance. Atmospheric Environment. 2008;42:9041-51.

[37] Tominaga Y. Visualization of city breathability based on CFD technique: case study for urban blocks in Niigata City. J Vis. 2012;15:269-76.

[38] Liu C-H, Leung DYC, Barth MC. On the prediction of air and pollutant exchange rates in street canyons of different aspect ratios using large-eddy simulation. Atmospheric Environment. 2005;39:1567-74.

[39] Hang J, Li Y. Ventilation strategy and air change rates in idealized high-rise compact urban areas. Building and Environment. 2010;45:2754-67.

[40] Lin M, Hang J, Li Y, Luo Z, Sandberg M. Quantitative ventilation assessments of idealized urban canopy layers with various urban layouts and the same building packing density. Building and Environment. 2014;79:152-67.

[41] Wong MS, Nichol J, Ng E. A study of the “wall effect” caused by proliferation of high-rise buildings using GIS techniques. Landscape and Urban Planning. 2011;102:245-53.

[42] Yim SHL, Fung JCH, Lau AKH, Kot SC. Air ventilation impacts of the “wall effect” resulting from the alignment of high-rise buildings. Atmospheric Environment. 2009;43:4982-94.

[43] Hang J, Sandberg M, Li Y, Claesson L. Pollutant dispersion in idealized city models with different urban morphologies. Atmospheric Environment. 2009;43:6011-25.

[44] Blocken B. Computational Fluid Dynamics for urban physics: Importance, scales, possibilities, limitations and ten tips and tricks towards accurate and reliable simulations. Building and Environment. 2015;91:219-45.

[45] Salim SM, Buccolieri R, Chan A, Di Sabatino S. Numerical simulation of atmospheric pollutant dispersion in an urban street canyon: Comparison between RANS and LES. Journal of Wind Engineering and Industrial Aerodynamics. 2011;99:103-13.

[46] Sandberg M. The multi-chamber theory reconsidered from the viewpoint of air quality studies. Building and Environment. 1984;19:221-33.

[47] Bady M, Kato S, Huang H. Towards the application of indoor ventilation efficiency indices to evaluate the air quality of urban areas. BAE Building and Environment. 2008;43:1991-2004.

[48] Michael J. Brown, Robert E. Lawson, David S. DeCroix, Lee RL. Comparison of Centerline Velocity Measurements Obtained Around 2D and 3D Building Arrays in a Wind Tunnel. International Society of Environmental Hydraulics Conf. Tempe, AZ2001.

[49] Franke J, Baklanov A. Best practice guideline for the CFD simulation of flows in the urban environment COST action 732 Quality assurance and improvement of microscale meteorological models. Hamburg: Meteorological Inst.; 2007.

[50] Tominaga Y, Mochida A, Yoshie R, Kataoka H, Nozu T, Yoshikawa M, et al. AIJ guidelines for practical applications of CFD to pedestrian wind environment around buildings. Journal of Wind Engineering and Industrial Aerodynamics. 2008;96:1749-61.

[51] Bolger N, Amarel D. Effects of social support visibility on adjustment to stress: Experimental evidence. Journal of Personality and Social Psychology. 2007;92:458-75.

[52] Blocken B, Stathopoulos T, Carmeliet J. CFD simulation of the atmospheric boundary layer: wall function problems. Atmospheric Environment. 2007;41:238-52.

[53] Hargreaves DM, Wright NG. On the use of the k‐ model in commercial CFD software to model the neutral atmospheric boundary layer. Journal of Wind Engineering and Industrial Aerodynamics. 2007;95:355-69.

[54] Blocken B, Stathopoulos T, Saathoff P, Wang X. Numerical evaluation of pollutant dispersion in the built environment: Comparisons between models and experiments. Journal of Wind Engineering and Industrial Aerodynamics. 2008;96:1817-31.

[55] Gousseau P, Blocken B, Stathopoulos T, van Heijst GJF. CFD simulation of near-field pollutant dispersion on a high-resolution grid: A case study by LES and RANS for a building group in downtown Montreal. Atmospheric Environment. 2011;45:428-38.

[56] Gousseau P, Blocken B, van Heijst GJF. CFD simulation of pollutant dispersion around isolated buildings: On the role of convective and turbulent mass fluxes in the prediction accuracy. Journal of Hazardous Materials. 2011;194:422-34.

[57] van Hooff T, Blocken B. CFD evaluation of natural ventilation of indoor environments by the concentration decay method: CO2 gas dispersion from a semi-enclosed stadium. Building and Environment. 2013;61:1-17.

[58] Blocken B, Vervoort R, van Hooff T. Reduction of outdoor particulate matter concentrations by local removal in semi-enclosed parking garages: A preliminary case study for Eindhoven city center. Journal of Wind Engineering and Industrial Aerodynamics. 2016;159:80-98.

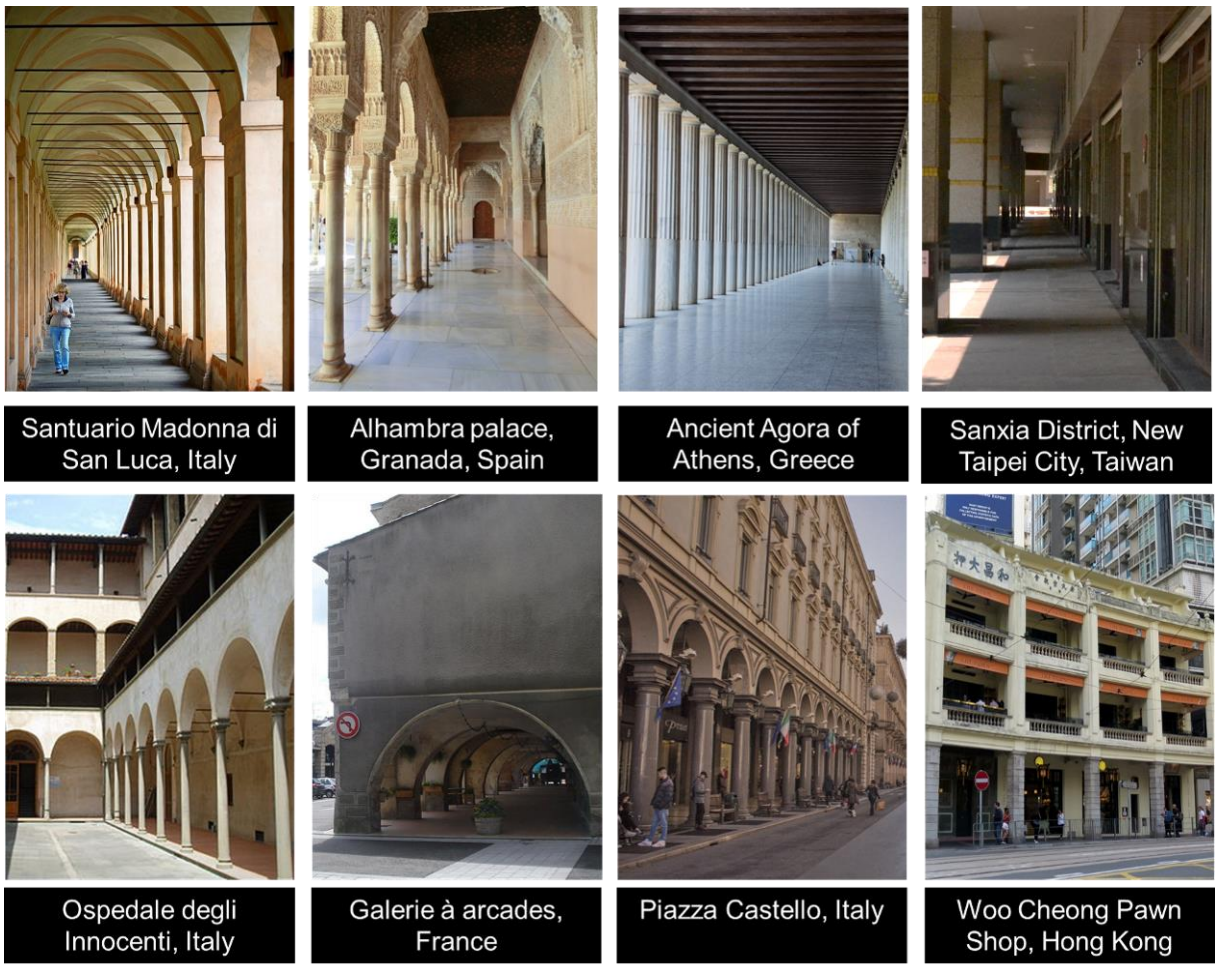

Figure 1 Photos of various arcade designs as half-open spaces of buildings in realistic urban areas (photographed by Wikipedia).

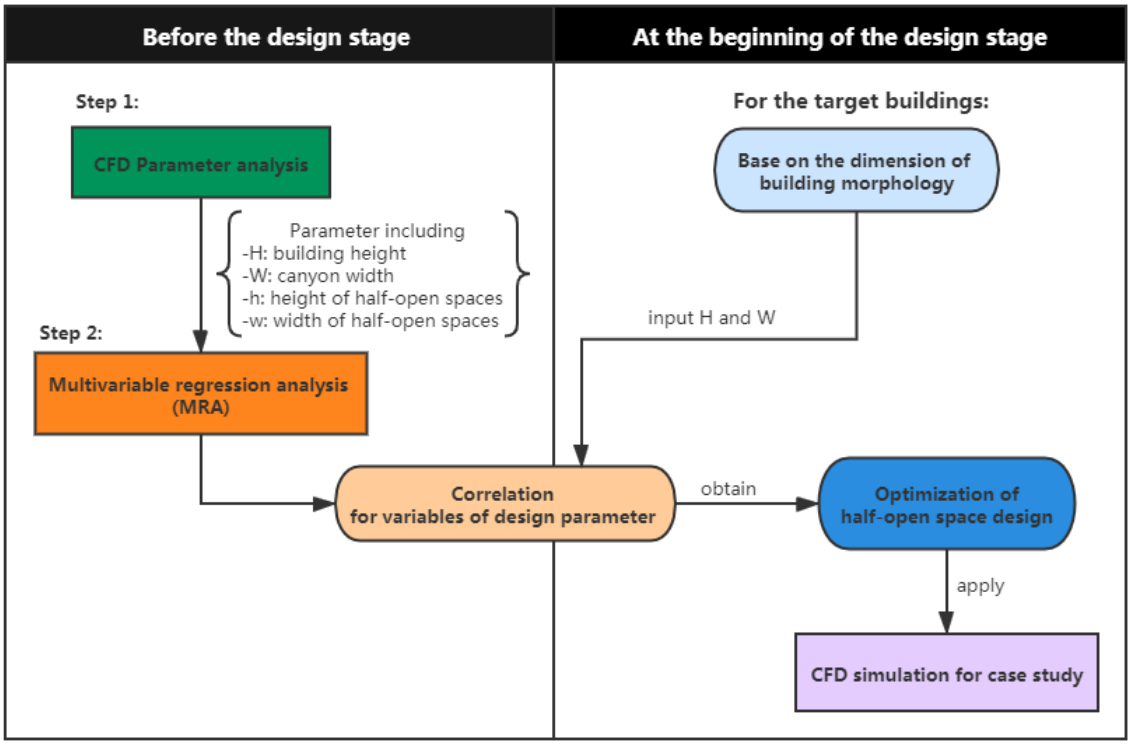

Figure 2 Schematic illustrating the combined framework and its application to target buildings.

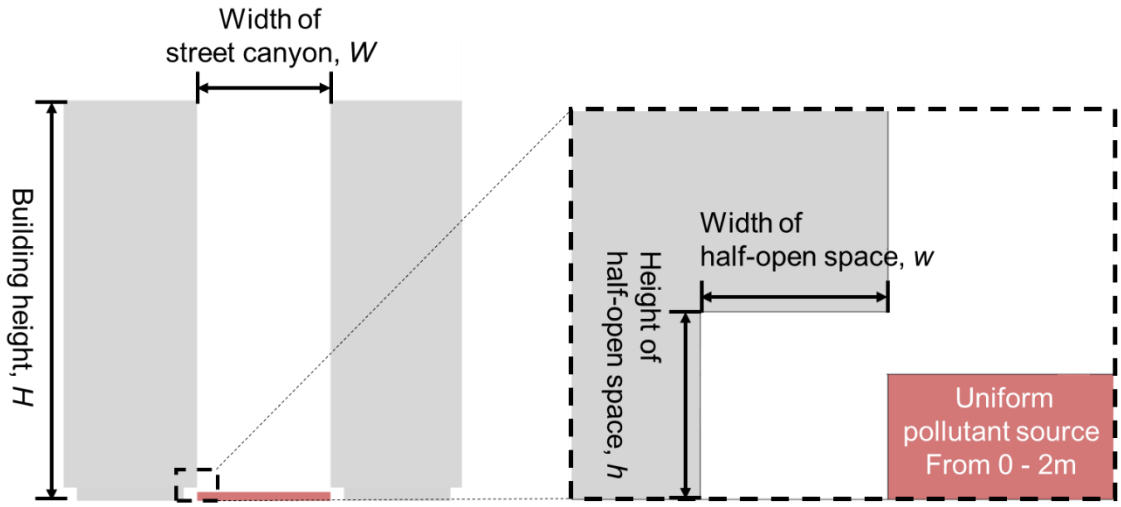

Figure 3 Schematic of four parameters of half-open space in ideal street canyons.

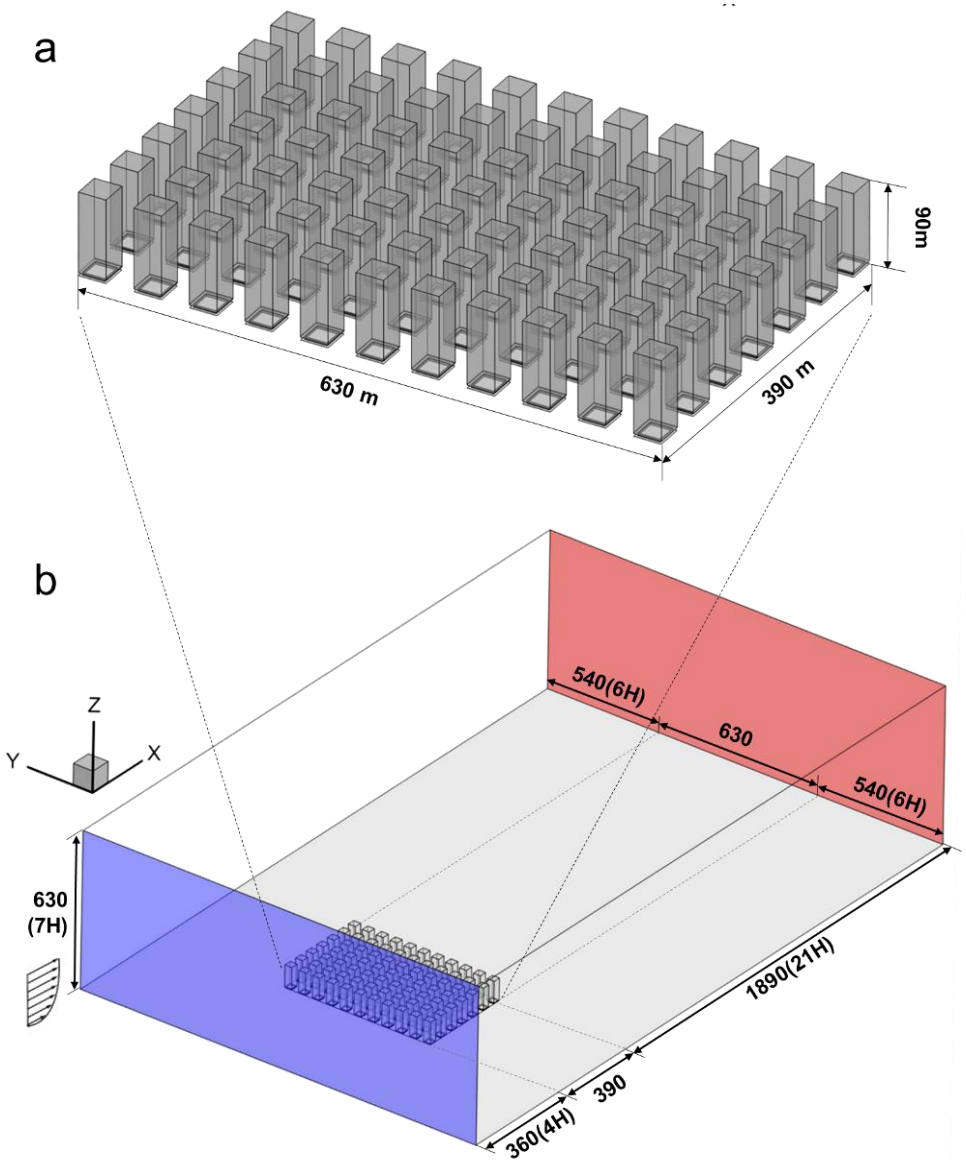

Figure 4 (a) Geometries of 3D idealized high-rise building array and (b) computational domain.

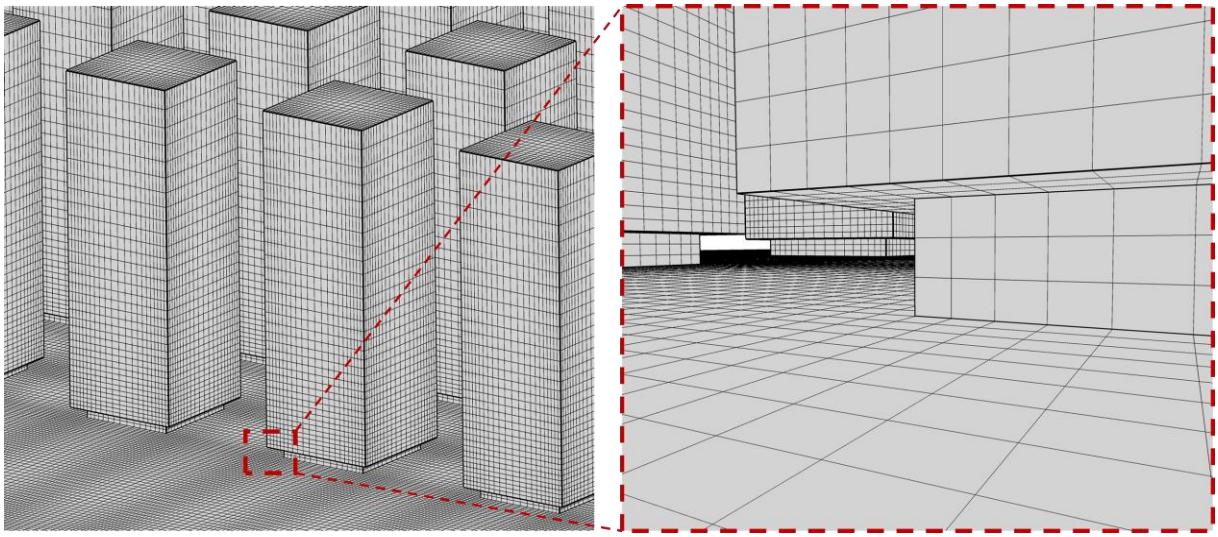

Figure 5 Computational grids at surfaces of high-rise building model and half-open space in an enlarged view

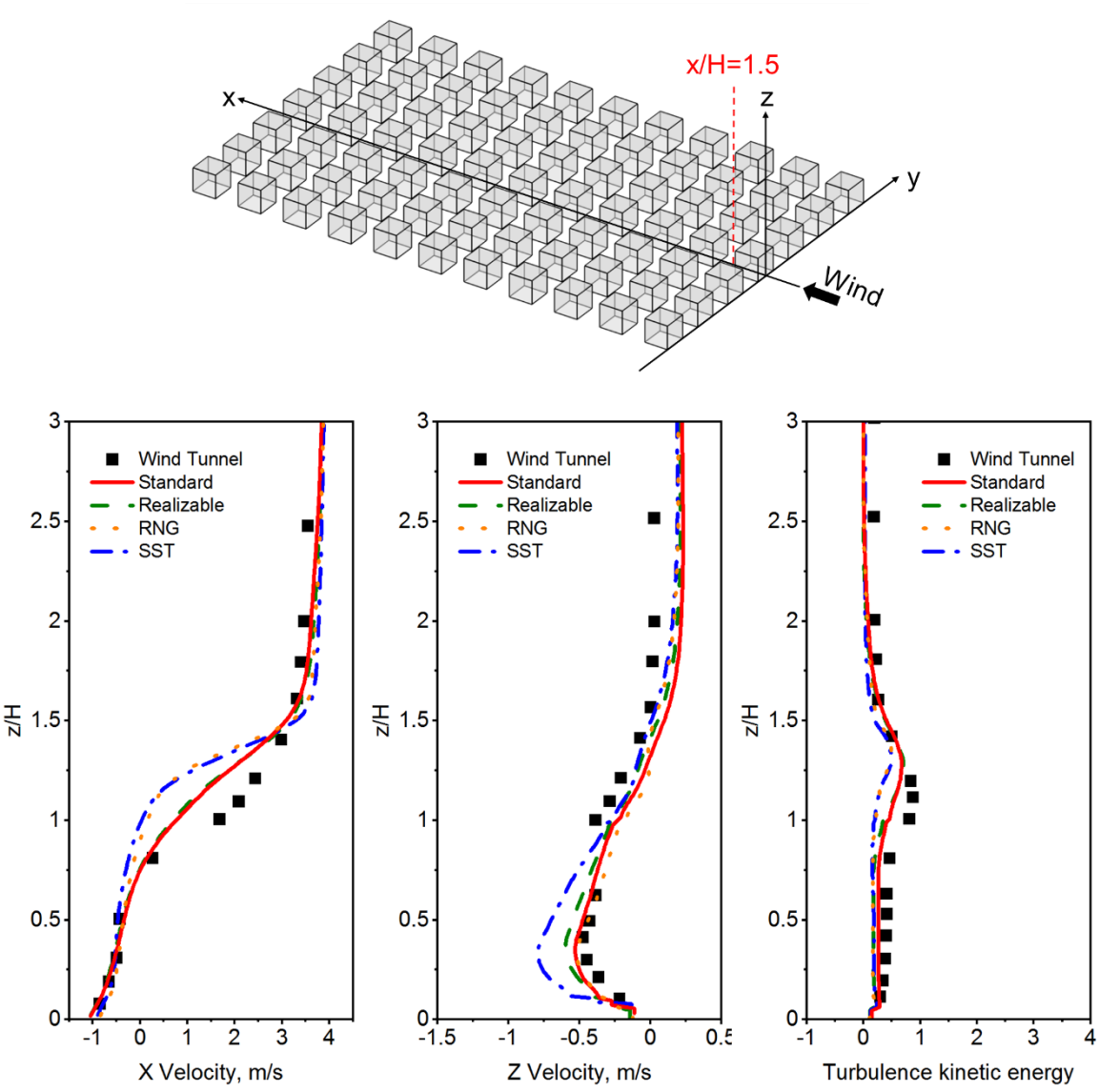

Figure 6 Comparison of CFD predictions with wind-tunnel measurements of X velocity, Z velocity and turbulence kinetic energy at x/H= 1.5 for a generic building array.

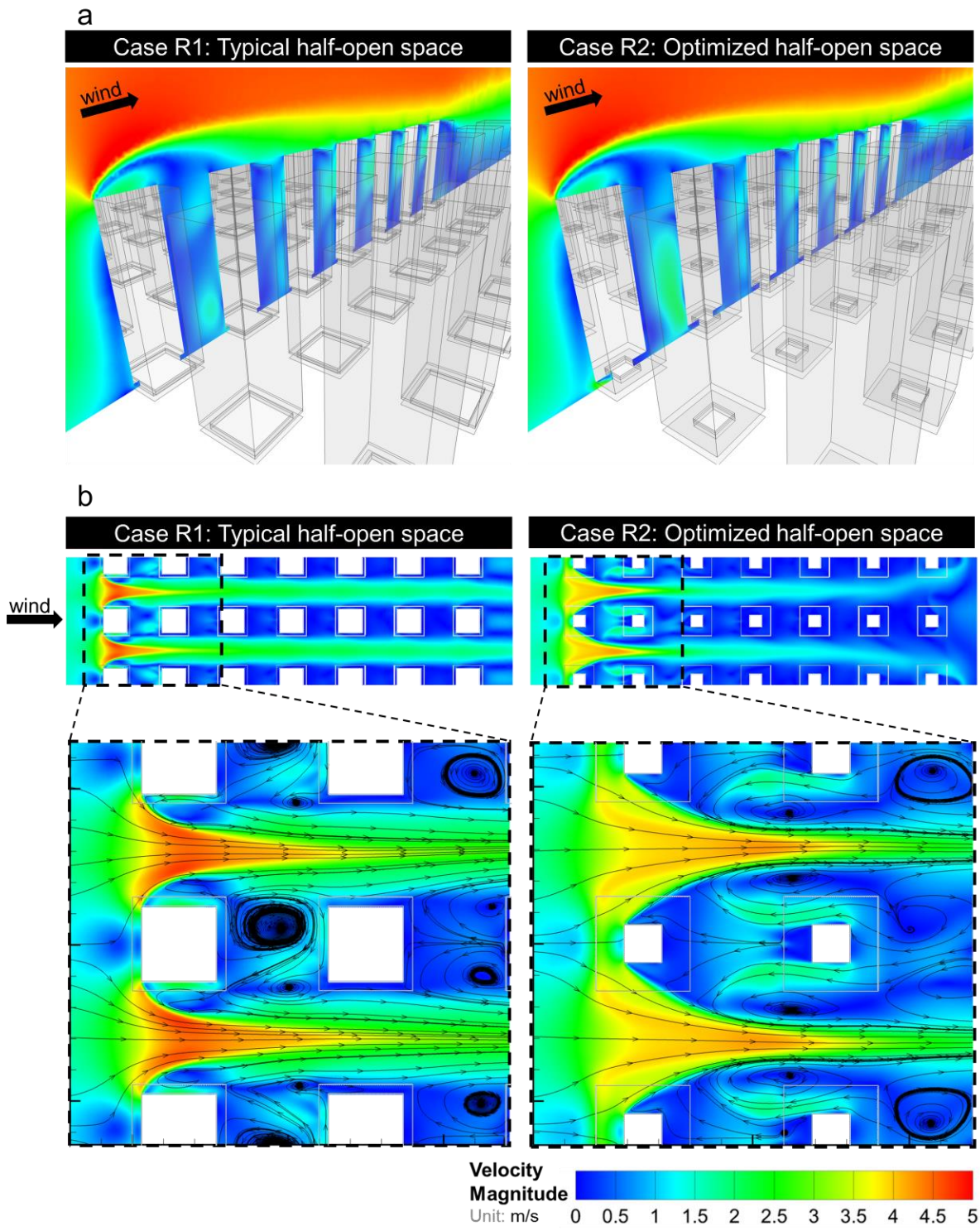

Figure 7 Predicted velocity magnitude contours in (a) vertical cross-sectional plane of Y= 0 m and (b) horizontal cross-sectional plane at a pedestrian height of Z= 1.75 m for typical (Case 1) and optimized (Case 2) half-open space layouts.

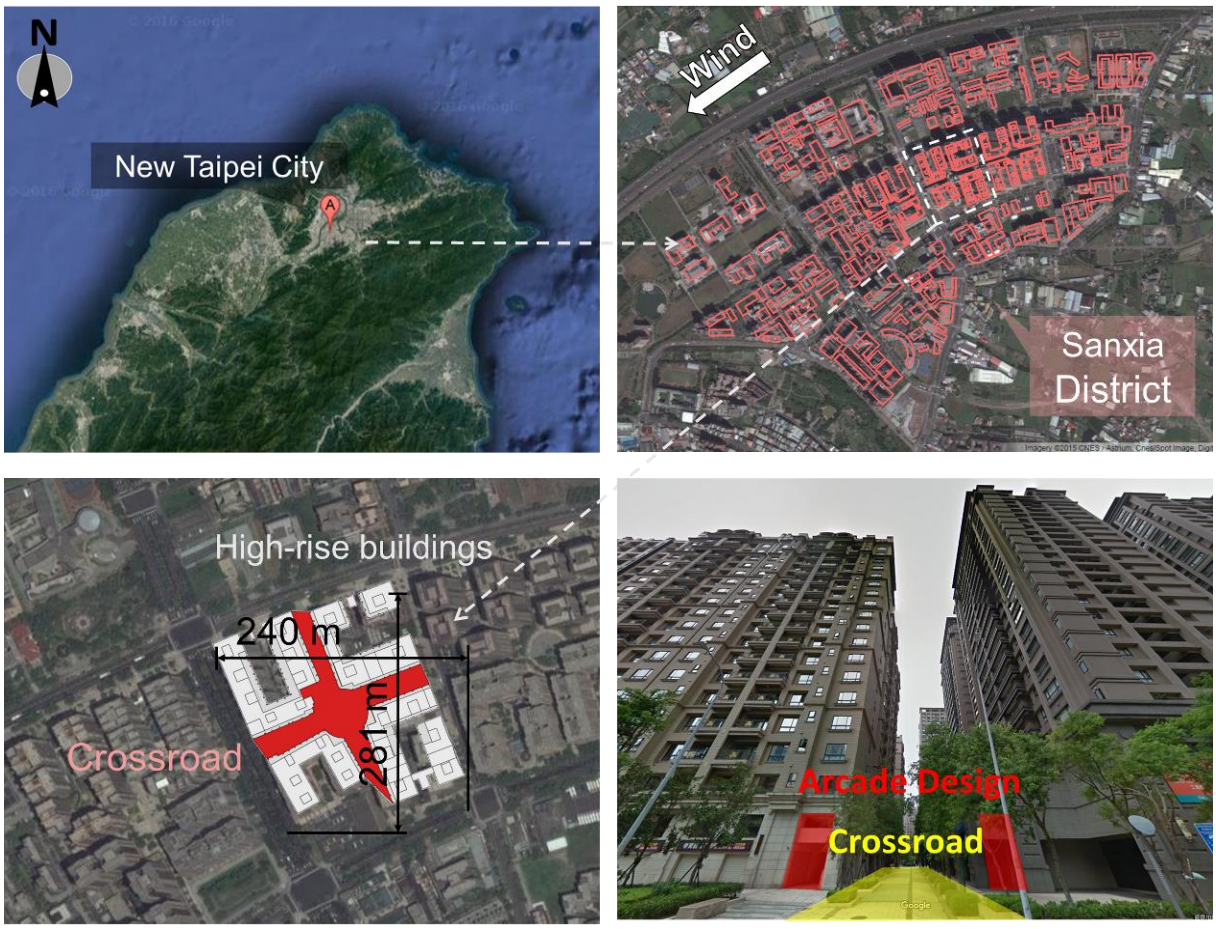

Figure 8 Location and pictures of studied site with high-rise building models of crossroad in realistic high-rise urban areas

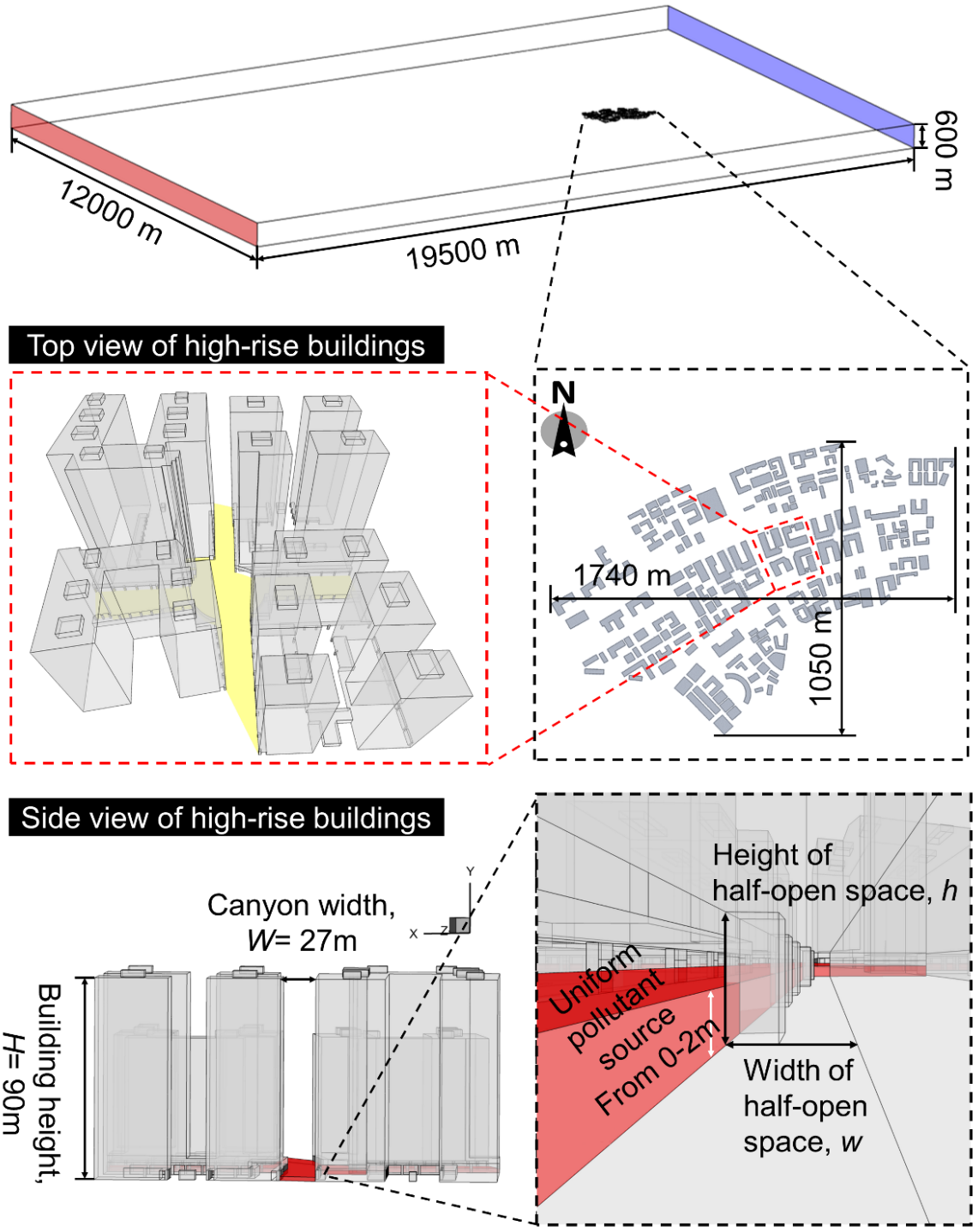

Figure 9 Computational domain, geometries of realistic high-rise urban areas with half-open space design.

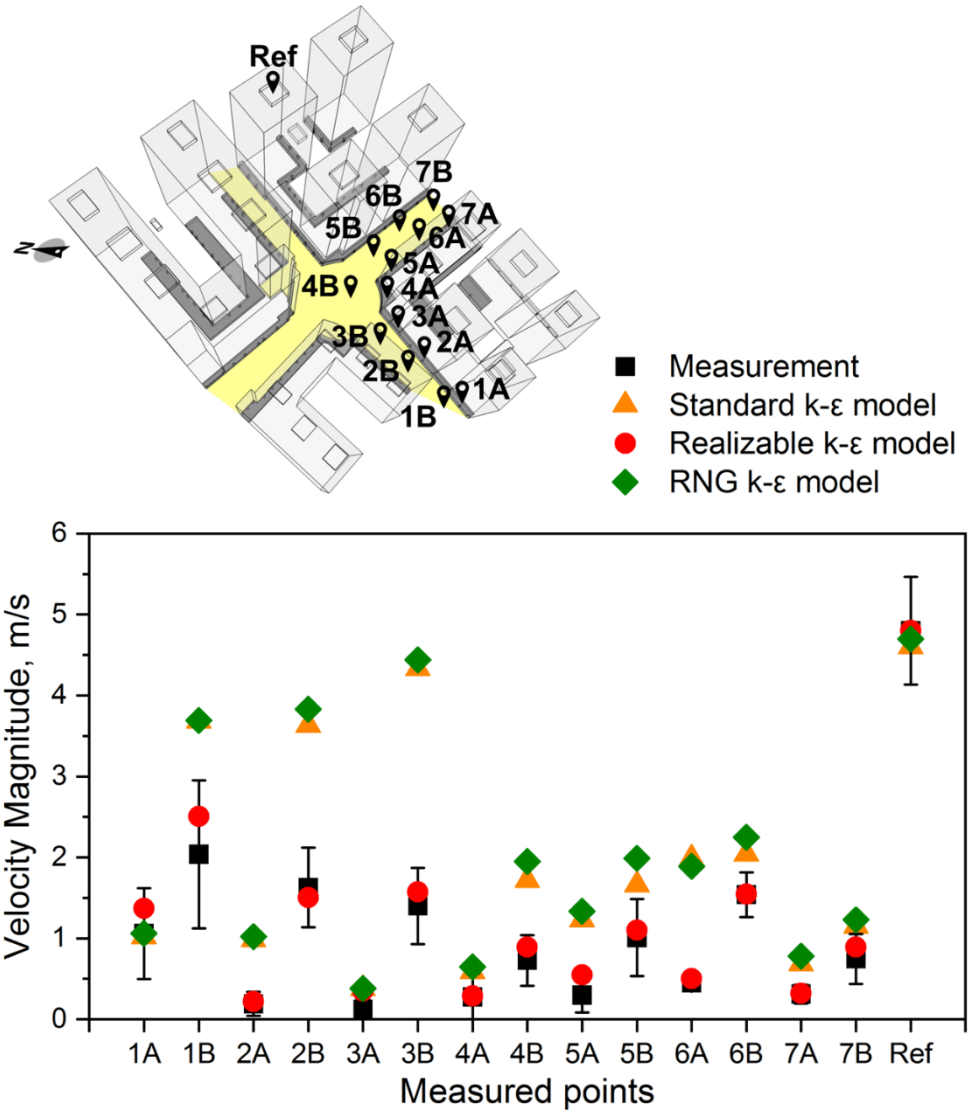

Figure 10 Comparison of CFD predictions with on-site measurements of velocity magnitude distributions for realistic case study.

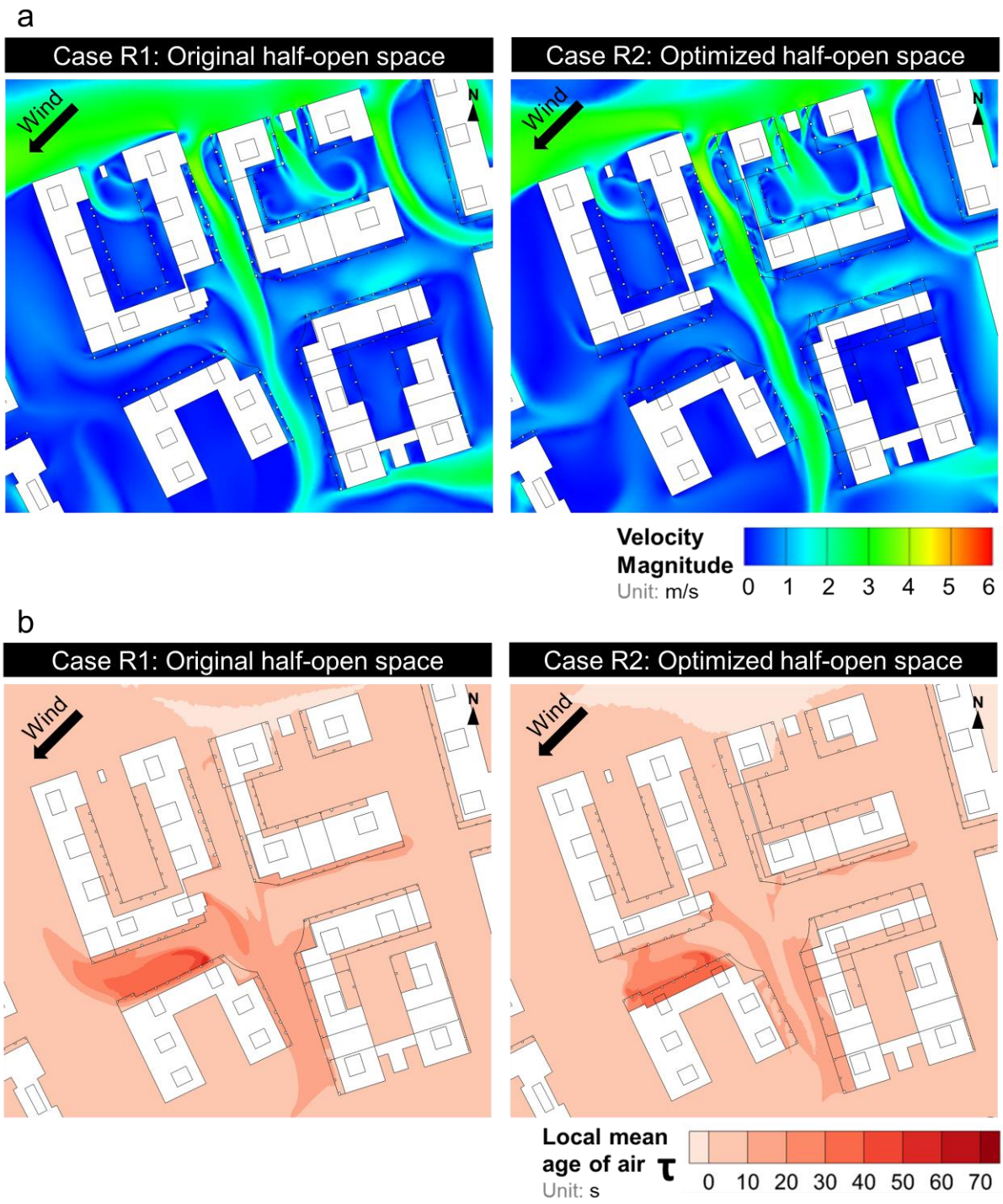

Figure 11 Predicted contours of (a) velocity magnitude and (b) local mean age of airin horizontal cross-sectional plane at a pedestrian height of Z=1.75 m for original (Case R1) and optimized (Case R2) half-open space layouts.

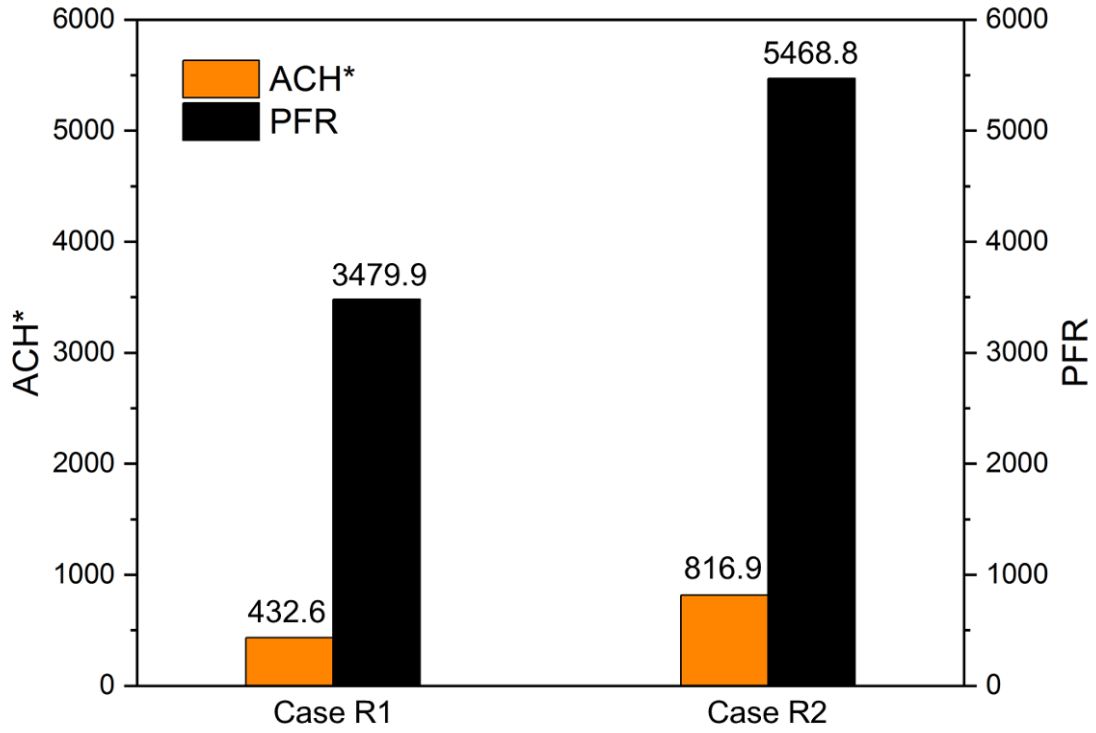

Figure 12Computed *ACH** and *PFR* outcomes for original (Case R1) and optimized (Case R2) half-open space layouts.